

Catalytic performance of carbon nanotubes in H₂O₂ decomposition: experimental and quantum chemical study

*K. Voitko¹, A. Tóth², E. Demianenko¹, G. Dobos³, B. Berke²,
O. Bakalinska¹, A. Grebenyuk¹, E. Tombácz⁴, V. Kuts¹, Yu. Tarasenko¹, M. Kartel,¹ K. László^{2*}*

¹ O.O. Chuiko Institute of Surface Chemistry of NAS of Ukraine, 17 General Naumov st.,
Kyiv, 03164, Ukraine

² Department of Physical Chemistry and Materials Science, Budapest University of Technology and
Economics, H-1521 Budapest, Hungary

³ Department of Atomic Physics, Budapest University of Technology and Economics, H-
1521 Budapest, Hungary

⁴ Department of Physical Chemistry and Materials Science, University of Szeged, H-6720 Szeged,
Aradi Vértanúk tere 1., Hungary

Abstract: The catalytic performance of multi-walled carbon nanotubes (MWCNTs) with different surface chemistry was studied in the decomposition reaction of H₂O₂ at various values of pH and temperature. A comparative analysis of experimental and quantum chemical calculation results is given. It has been shown that both the lowest calculated activation energy (~18.9 kJ/mol) and the highest rate constant correspond to the N-containing CNT. The calculated chemisorption energy values correlate with the operation stability of MWCNTs. Based on the proposed quantum chemical model it was found that the catalytic activity of carbon materials in electron transfer reactions is controlled by their electron donor capability.

Keywords: Functionalized MWCNT, heterogeneous catalysts, hydrogen peroxide decomposition, quantum chemical simulation

1. Introduction

Among the carbon materials that are widely used as heterogeneous catalysts [1] carbon nanotubes (CNTs) have been taking a key position since their discovery in 1991 [2]. These nano-scale carbon materials opened new possibilities in this area. Besides serving as a support, CNTs alone can be used as catalysts for some specific reactions, including methane and NO_x decomposition [3,4], oxidative dehydrogenization of aromatic hydrocarbons and alkanes [5-9], oxidation of aniline [10], p-toluidine [11], and benzyl alcohol [12], catalytic wet air oxidation of phenol [13,14] and p-coumaric acid [15,16], aerobic oxidation of cyclohexane [17,18], ozonation of oxalic acid [19,20], selective oxidation of H₂S [21], and heterogeneous hydroxylation of organics

[22]. Nitrogen-doped CNTs were used as basic catalyst in Knoevenagel condensation [23] and CO oxidation [24] reactions. Based on these results, it is very reasonable to conclude that CNTs can serve as an excellent heterogeneous catalyst having (1) the potential to form a macrostructured catalyst of sufficient mechanical strength; (2) a tunable morphology and surface chemistry for enhanced catalytic activity and selectivity; (3) high surface area and specific porosity; (4) good thermal stability and resistance against acidic/basic environment.

One of the widely used test reactions for studying the catalytic properties of carbon materials is hydrogen peroxide decomposition (HPD). Until now H_2O_2 has been used for the oxidation and purification of CNTs [25-27]. Oxidation under mild conditions (e.g., 15% H_2O_2 , 100°C, 3 hrs [27]) leads to shortened and uncapped CNTs with carboxylic groups on their surface. Nevertheless, it is well known that HPD is one of the oldest reactions found to be catalyzed by carbon materials, especially by activated carbons [28,29]. Earlier, it was found that CNT, compared to graphene and activated carbon, is also able to catalyze HPD [30]. Despite numerous investigations, the mechanism of this reaction is still not completely understood.

The activity of carbon catalysts in the HPD process is associated with the presence of delocalized π -electrons in the surface conjugated system. It is known that incorporation of heteroatoms (B, N, O) into the carbon matrix leads to changes in its adsorptive, catalytic, and electrochemical properties [31] due to the change the electron work function value at the carbon-fluid interface. The interaction between the π -electrons of the conjugated heteroatom containing system and the condensed carbon network defines the energetic characteristics of frontier molecular orbitals and controls the catalytic properties of carbon materials. It was found that the insertion of nitrogen atoms into the graphene lattice significantly enhances the HPD process by lowering the electron work function value from the carbonaceous surface and decreasing the band gap, thus producing higher electron mobility [32]. By contrast, insertion of oxygen-containing groups reduces the activity of carbon catalysts in HPD; moreover, samples having a high number of such groups do not catalyze the reaction [33].

Decomposition of hydrogen peroxide over a solid surface is a complex homolytic chain process [29,34]. One of the radical mechanism, the limiting step of this reaction is the disintegration of H_2O_2 molecule into two HO^\bullet radicals. The other is an ionic decomposition process, the dissociation of H_2O_2 as a weak acid ($\text{H}_2\text{O}_2 \rightleftharpoons \text{H}^+ + \text{OOH}^-$, $\text{pK}_a = 11.6$) [29]. Both are influenced by the solution pH condition, the presence of catalytic ions (e.g., Fe^{3+} , Γ) and also the surface chemistry of carbon

derivatives such as activated carbon in paper [29]. Since experimental investigation of the effect of the electron structure of CNT on the interaction with HO[•] radicals is difficult, quantum-chemical calculations are more appropriate.

This paper focuses on the activity of nitrogen- and oxygen-containing MWCNTs in HPD. Experimental results are supported by quantum chemical calculations that consider the electron structure, the thermodynamic and the activation characteristics in the HO[•] radical - CNT model cluster interaction.

2. Materials and methods

2.1. Carbon nanotubes

Pristine multi-walled carbon nanotubes (O.O. Chuiko Institute of Surface Chemistry of NAS of Ukraine) were synthesized by CVD method from a mixture of propylene and hydrogen using a mixed Al-, Fe-, and Mo-oxide catalyst [36]. After removing the accessible catalyst with HCl and NH₄F solutions the MWCNTs were washed with distilled water to neutral pH. The samples were kept at 748 K for 1 hr in air to reduce the amorphous carbon from 70 % to 3 %. From low temperature nitrogen adsorption the apparent surface area of the purified MWCNT is 162 m²/g, with outer diameter and wall thickness of 50-62 nm and 10-15 nm, respectively. The surface composition, estimated from XPS, is: 96.4 at% C, 3.6 at % O.

The purified CNT samples were oxidized in 70 % HNO₃ at 373 K for 4 hrs and then washed with distilled water and NaOH solution for 12 hrs [37]. After washing again to neutral pH, the acidic sites were regenerated with 0.1 M HCl solution. The oven-dried (378 K, 4 hrs) nanotubes are labeled as O-CNT. Nitrogen was introduced by treating O-CNT with 10 v/v% urea solution. Drying and further heat treatment in Ar atmosphere (973-1073 K, 1 hr) yielded N-CNT. No further purification was applied.

2.2. Characterization methods

Low temperature (77.4 K) nitrogen adsorption/desorption isotherms were measured using a NOVA 2000e (Quantachrome) automatic analyzer. The samples were evacuated at 293 K for 24 h. The specific surface area (S_{BET}) was calculated according to the BET method.

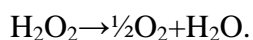
Continuous potentiometric titration over the pH range of 3 to 11 was performed in a CO₂-free medium to determine the specific amount of net proton surface excess (Δn^{σ} , mmol/g), i.e., the

difference between the surface excess amounts of H^+ ($n_{H^+}^\sigma$) and OH^- ($n_{OH^-}^\sigma$) [38]. The MWCNTs were suspended in 0.01 M NaCl solution prepared from freshly produced Millipore water and ultrasonicated for 15 min. 0.1 M HCl and 0.1 M NaOH solutions were used respectively to titrate the surface from the pH of immersion down to pH 3, then up to pH 10. Experimental details are given in [39].

The surface chemical composition of the samples was determined by X-ray photoelectron spectroscopy (XPS) using an XR3E2 twin anode X-ray source (300 W, VG Microtech) and a Clam2 hemispherical electron energy analyzer. The base pressure of the analysis chamber was about 5×10^{-9} mbar. Samples were analysed using a $MgK\alpha$ (1253.6 eV) anode, without monochromatization. Wide scan spectra in the binding energy range 0 – 1100 eV were measured with an energy band-pass of 50 eV for all the samples. High-resolution spectra of the C1s, O1s and N1s signals were recorded in 0.05 eV steps with energy band-pass 20 eV. The peak fitting procedure was performed with the CasaXPS program (Version 2.19). After subtraction of a Shirley type base line, curve fitting was carried out assuming a combined Gaussian (70%) and Lorentzian (30%) peak shape. This technique probes the sample composition to a depth of a few nanometers.

2.3. Catalytic activity in HPD reaction

The catalytic activity of the O-CNT and N-CNT samples was detected by measuring the volume of released oxygen in the following overall reaction:



The HPD was conducted in the concentration range of 0.2-1.2 vol.% and 4-10 vol.% for N-CNT (mass of the sample 0.005 g) and O-CNT (mass of the sample 0.05 g), respectively. These conditions were optimized in previous preliminary experiments [30].

The MWCNT samples were sonicated in the corresponding phosphate buffer ($Na_2HPO_4 + KH_2PO_4$, Sigma) for 15 minutes. After that, aqueous H_2O_2 (Sigma, 50% vol.%) solution was added to the suspension (total reaction volume 25 ml) and stirred for 30 minutes. The initial pH and the temperature were varied in ranges of 4.5 to 8.0 and 293-323 K respectively. The volume of the released oxygen (0.05 to 5 ml, +/-0.01 ml) was measured in a microburette. In a blank experiment without nanotubes the oxygen yield was below the detection limit in all the cases. The total O_2 yield can therefore be attributed to the H_2O_2 decomposition over the nanotube surfaces.

For analysis, quantitative assessment, and comparison of the activity of O-CNT and N-CNT, the rate constant (k , s^{-1}) and activation energy (E_a , kJ/mol) were determined as described below.

The reaction rate r of the catalytic process can be described by the equation $r = k[H_2O_2]_0^n m^n$, where $[H_2O_2]_0$ is the initial concentration of the hydrogen peroxide, m is the mass of the catalyst and n is the reaction order. If m is constant and $n=1$, then

$$\log r = \log k + n \log[H_2O_2]_0 \quad (1).$$

By plotting the data in the form $y=ax+b$, k was determined as $k=10^b$, as illustrated in Figure 1. Similar calculations were performed for all the systems studied.

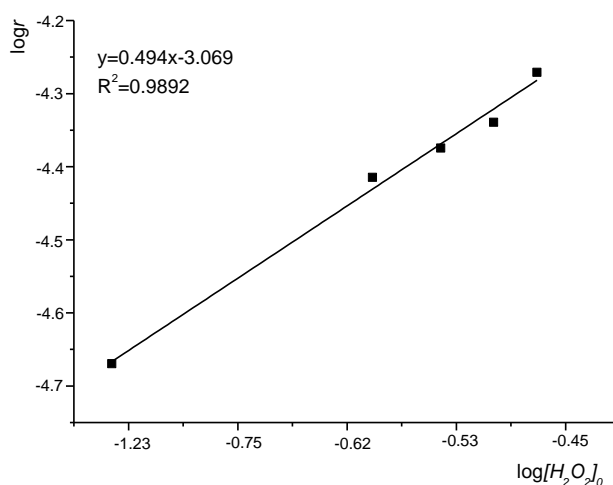


Figure 1. Determination of the rate constant; N-CNT at pH~8.0.

An important characteristic of any catalyst is its operational stability (stability over repeated reaction cycles) which allows them to be reused as eco-friendly, cost-effective, and energy-efficient catalysts without additional regeneration. The operational stability of the CNTs was examined over 10 cycles (30 min each) at 298 K. The samples were placed in contact with H_2O_2 solution for 30 min, then separated by means of a cellulose membrane (Amicon 8200 cylindrical ultrafiltration cell, Millipore, USA), washed, and dried. The cycle was repeated 10 times with fresh H_2O_2 solutions. Before each step, the pH was set as stated in the caption.

2.4. Quantum-chemical calculations

The density functional theory (DFT) is widely used for the calculation of nanotube properties [24]. Among the DFT methods a hybrid method such as B3LYP is a good choice since it shows

excellent agreement with the experimental data [40,41]. To ascertain the mechanism of the influence of the electronic nature of the CNTs on HPD, the thermodynamic and kinetic characteristics of the HO[•] radical - carbon cluster interaction were calculated. The calculation was performed using the DFT method with B3LYP exchange-correlation functional and 6-31G (d,p) basis set [42,43]. The dispersion correction was taken into account using the DFT-D3 program package by Grimme et al. [44]. The effect of the aqueous environment was simulated within the supermolecular approximation and within the continuous solvent model (CPCM), using the US GAMESS program package [45]. The stationary character of the minimum energy structures obtained and the presence of transition states were proved according to the Murrell-Laidler theorem with additional calculation of Hessian matrices [46]. This enabled us to define the thermodynamic free energy of physical (ΔG_{pa}) and chemical (ΔG_{ca}) adsorption and the kinetic Gibbs free activation energy (ΔG_{act}) of HPD at 298 K [47]. A conjugated π -system of a graphene layer with 14 condensed rings was used to simulate a part of the CNT surface (Figure. 2). In order to clarify whether chemical or structural factors affect the energetics of addition of the hydroxyl radical, four nanoclusters (NCs) were considered. The nitrogen-containing nanotubes may have both amino groups and quaternary nitrogen atoms while the oxygen atom may be present in hydroxyl, carboxyl and epoxy groups (Figure 2).

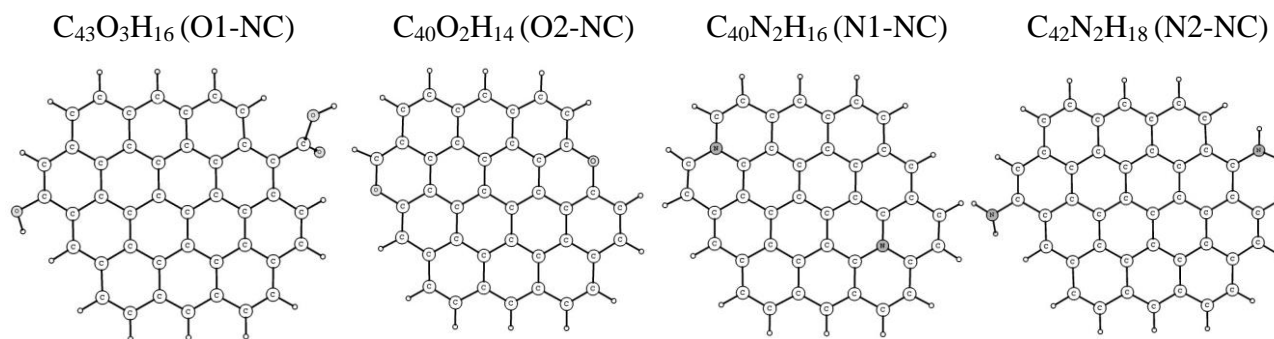


Figure 2. Structure of the oxygen- and nitrogen-containing model clusters.

Table 1. Energy characteristics of the model nanoclusters

Nanocluster	$-E_{HOMO}$, eV	$-E_{LUMO}$, eV
O1-NC	4.773	2.357
O2-NC	4.063	1.813
N1-NC	3.205	1.739
N2-NC	4.024	1.758

These clusters were selected in view of the large diameter of the CNTs examined (50-62 nm). The $[C_{43}O_3H_{16}]$ and $[C_{40}N_2H_{16}]$ nanoclusters are represented as planar matrices with sp^2 -hybridized carbon atoms; the concentrations of the heteroatoms in the model NCs are close to the that of O- and N-atoms in the O-CNT and N-CNT samples detected by XPS [30]. The calculated energy characteristics of the selected NCs are listed in Table 1, where E_{HOMO} is the energy of the highest occupied molecular orbital and E_{LUMO} is the energy of the lowest unoccupied molecular orbital.

3. Results and discussion

3.1. Experimental section

Figure 3 shows the kinetic curves of H_2O_2 decomposition in the presence of the samples investigated. The oxidized sample (O-CNT) has a low catalytic activity and an approximately linear curve different from that of the nitrogen-doped (N-CNT). As the initial sample [30] hardly exhibits any catalytic capability toward HPD the enhanced activity of the oxidized nanotubes may arise from the morphological and surface chemical changes induced by the oxidation process. The nitric acid attacks the carbon layers, resulting in sidewall damage and incidentally opening access to the inner bores [48,49]. The oxidation introduces new surface functional groups into the edges and defects, modifying at the same time the density distribution of the delocalized electrons. Moreover, as electron donor/acceptor sites are strong free radical scavengers [28,50], the free radicals from H_2O_2 may adsorb and become deactivated on the surface of the MWCNT. The acidic oxidation disrupts the delocalized π -electron network, which can suppress the surface deactivation capability. Thus OH^\bullet radicals can maintain the decomposition reaction.

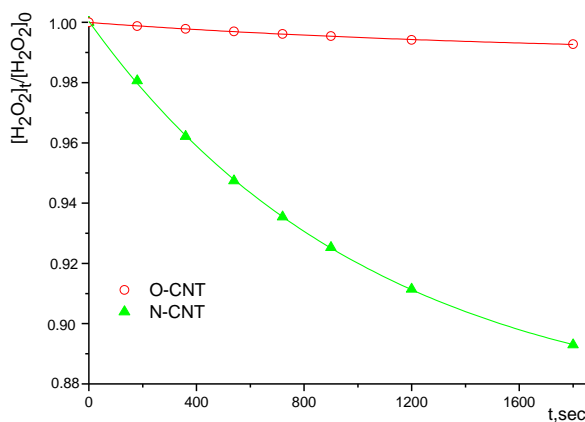


Figure 3. Kinetic curves of H₂O₂ decomposition on O-CNT ([H₂O₂]₀=2.35 mol/l) and N-CNT ([H₂O₂]₀=0.235 mol/l) at 293 K, pH~8.0.

In contrast to O-CNT, the nitrogen-containing sample exhibits rather good activity and decomposes 10% of H₂O₂ within 30 minutes.

To explain the results obtained we used the quantum-chemical approach developed in references [31, 32], which describes the relationship between the number and the position of N-atoms in the graphene planes and their energy parameters (energy values of the frontier molecular orbitals E_{HOMO} and E_{LUMO}). According to this concept, the positive effect of the nitrogen atoms on the catalytic properties of the CNTs in electron transfer reactions could be explained by a decrease in the band gap of the N-CNT, thus producing higher electron mobility and lowering the value of the electron work function at the N-CNT-H₂O₂ interface. Oxidation of CNTs leads to a decrease in their catalytic activity. Compared to N-CNT, O-CNT has a higher electron work function, and therefore the transfer of electrons to the hydrogen peroxide molecules is more difficult.

A series of experiments on HPD with CNT were carried out at various initial pH values in the range 4.5 to 8.0 (Figure. 4a). It has been found that N-CNT is three times more active than O-CNT in acidic and four times more active in alkaline media. With increasing pH the decomposition of H₂O₂ improved on both samples. Obviously, this tendency is connected on the one hand with the enhanced dissociation of H₂O₂ as a weak acid [29] and on the other hand with the changes in the charge state of the functionalized carbon surface. Figure 4b demonstrates that a relatively large proton excess accumulates on the N-CNT in acidic media, showing the dominance of positive basal plane charge due to the protonation reaction of basic sites such as amino groups and quaternary nitrogen atoms supposed in our quantum-chemical calculations, e.g., $CNT-NH_2 + H_3O^+ \rightleftharpoons CNT-NH_3^+ + H_2O$, which decreases as the pH rises. These protonated sites probably interact with the dissociation product OOH^- of H₂O₂, stabilizing it in adsorbed state and preventing oxygen evolution. The rate constant of the latter increases with increasing pH (Fig. 4a) in parallel with decreasing surface density of protonated sites (Fig. 4b). At the same time, N-CNT exhibits the highest activity in alkaline media, which indicates that a near neutral basal plane charge, where the amount of protonated N sites is roughly equal to that of deprotonated acidic sites, e.g., $CNT-COOH + H_2O \rightleftharpoons CNT-COO^- + H_3O^+$, is more active in HPD, since in this zwitterionic surface state OOH^- can no longer adsorb to the basic surface site. Moreover, in alkaline media the dissociation process $H_2O_2 \rightleftharpoons H^+ + OOH^-$ (pKa = 11.6) is enhanced by water formation ($H^+ + OH^- \rightleftharpoons H_2O$, log K ~14) and OOH^-

decomposes very readily, producing oxygen. In a weak acidic media O-containing surface groups (COOH, OH, HCO etc.) can form stable hydrogen bonds with H_2O_2 molecules, thereby inhibiting HPD. The presence of $-\text{COOH}$ groups on the surface retard the catalytic decomposition of H_2O_2 , since it suppresses dissociation under these conditions [29].

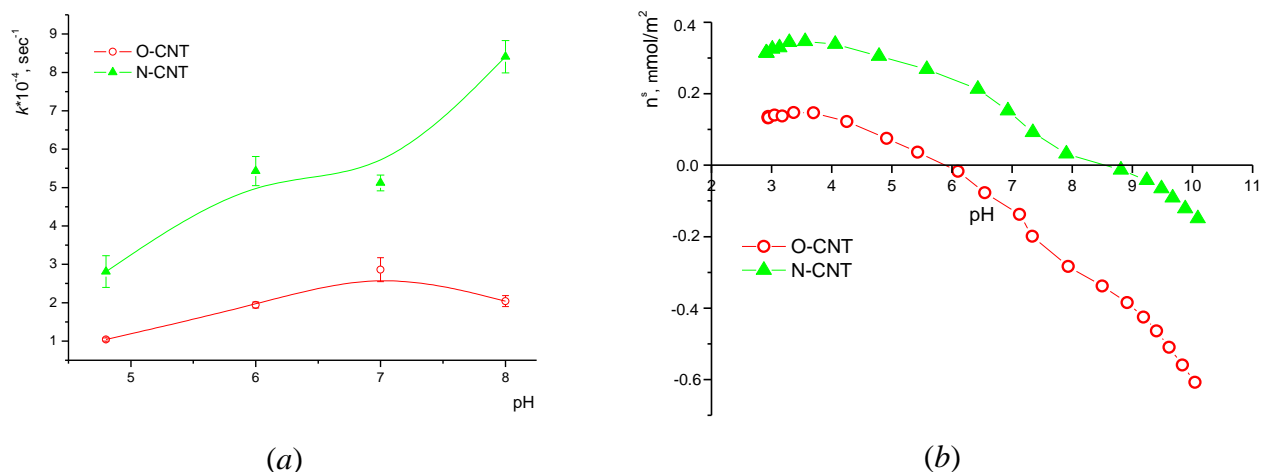


Figure 4. pH dependence of (a) decomposition of H_2O_2 on N-CNT ($[\text{H}_2\text{O}_2]=0.06\text{-}0.35 \text{ mol/l}$) and on O-CNT ($[\text{H}_2\text{O}_2]=0.6\text{-}3.5 \text{ mol/l}$) and (b) net proton surface excess from potentiometric titration (pH 3 \rightarrow pH 10).

The same correlation for O-CNT samples was observed until pH=7.0. At pH>7 the catalytic activity slightly decreases: the COOH groups convert into $[\text{COO}^-]$ form and thus affect the rate constant of HPD.

The activation energies characterizing the catalytic activity of the investigated CNTs between 293 and 323 K are presented in Figure 5. From the logarithmic Arrhenius plot the activation energy E_a is 27.4 ± 3.2 (O-CNT) and $15.4 \pm 2.8 \text{ kJ/mol}$ (N-CNT). These values indicate that the rate of HPD is limited not only by the reactions at the active surface sites, but also by the diffusion of the H_2O_2 molecules to these sites. It should be noted that the E_a values for oxidized and N-containing activated carbons are 57.5 and 29.2 kJ/mol respectively, showing a similar trend as our values. This similarity could be evidence of the same mechanism of HPD on carbon materials [51].

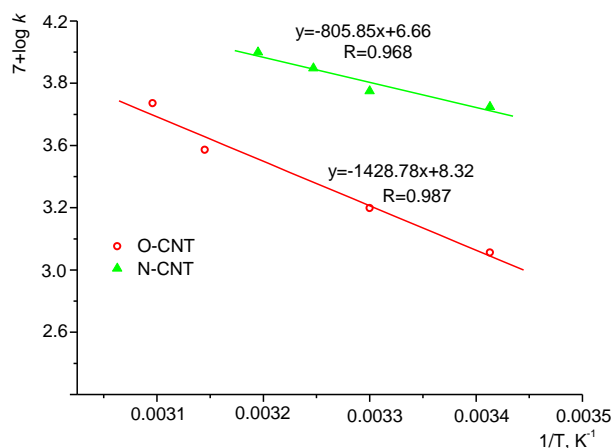


Figure 5. Arrhenius plot for the activation energy calculation of O-CNT (pH~6.9) and N-CNT (pH~8.0).

Figure 6 compares how the operation stability of investigated samples varied during the repeated cycles. The two kinds of nanotubes exhibit completely different behavior. It is observed that activity of the N-CNT decreases until the third cycle, a feature that may be associated with slow deactivation of the N-functionality in the carbon system. This fact was confirmed by XPS analysis (Table 2), detecting no nitrogen atoms in N-CNT after the third cycle. Between the fourth and sixth cycles the rate constant begins to stabilize, then the rate decreases further due to oxidative damage to the carbon lattice. The amounts of O-containing groups increased by a factor of almost 3.5, which proved our hypothesis.

Table 2. Surface composition from XPS (at.%) and the apparent surface area (m^2/g) of the MWCNTs before and after (*) 3rd catalytic cycle of HPD

Sample	XPS results						S_{BET}	S_{BET}^*
	$\text{C}1s$	$\text{C}1s^*$	$\text{O}1s$	$\text{O}1s^*$	$\text{N}1s$	$\text{N}1s^*$		
O-CNT	95.5	91.2	4.5	8.8	-	-	141	135
N-CNT	98.3	96.3	1.1	3.7	0.6	-	145	137

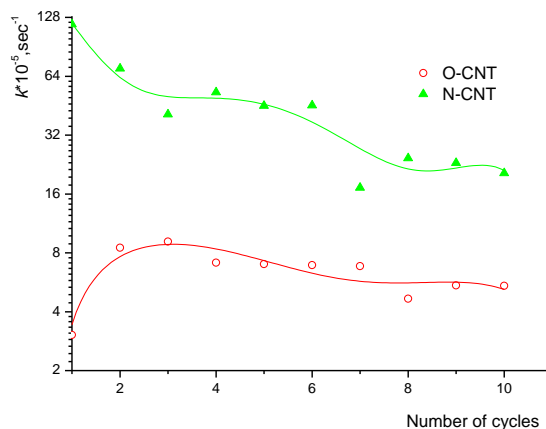


Figure 6. Operational stability of the O-CNT ($[\text{H}_2\text{O}_2]_0=1.47 \text{ mol/l}$, $\text{pH}\sim 6.9$) and N-CNT ($[\text{H}_2\text{O}_2]_0=0.235 \text{ mol/l}$, $\text{pH}\sim 8.0$).

Oxidation of the N-CNT surface was also confirmed by TPD analysis (Fig. 7). The appearance of an intense H_2O peak after the 3-rd cycle indicates enhanced surface hydrophilicity during the catalytic reaction. The adsorption of OH^- radicals on the CNT surface or the reaction of H_2O_2 with surface functional groups may result in this effect. The CO_2 evolution spectra (Fig. 7b) reveals that after three cycles the CO_2 peak corresponding to carboxyl groups (423–673 K), shifts toward higher temperatures (773–973 K) that corresponds to lactonic groups [52], which might be less active in HPD reaction.

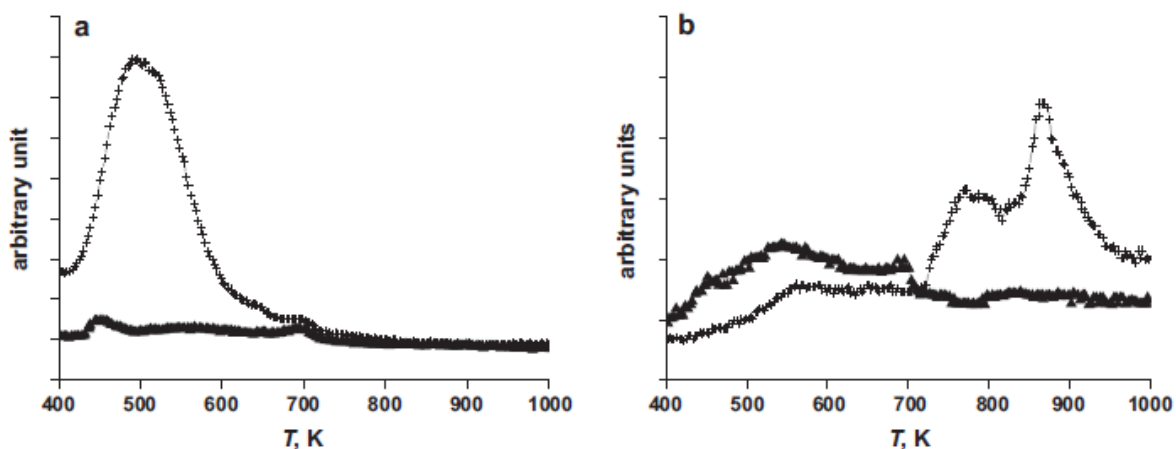


Figure 7. H_2O (a) and CO_2 (b) evolution in TPD spectra of N-CNT before (N) and after (+) the 3rd catalytic cycle of HPD.

The catalytic activity of the O-CNT slowly increases during three cycles due to the changes in surface chemistry. It was found that while there is practically no change in surface area, the surface chemistry exhibits significant changes. The XPS results indicate that the oxygen content doubles after the 3-rd cycle. At the same time the oxygen functionalities already present reduce the reactivity of O-CNT against further oxidation. We suggest that the active sites on the O-CNT surface are oxidatively removed by the H₂O₂, thus leaving other, less active acidic groups [30]. This hypothesis is also justified by the deconvoluted O 1s envelop of O-CNT (Table 3). The enhanced concentration of the C type oxygens (acids, esters, and hydroperoxides) and the appearance of peroxy groups (D type) indicate the oxidative change of the CNT surface during catalytic process.

Table 3. Surface composition from O 1s XPS of the O-CNT before and after (✓) 3rd catalytic cycle of HPD.

	Surface composition (at.%)	
	O 1s	O 1s*
A	0.5	1.2
B	2.6	2.8
C	1.4	4.1
D	0.0	0.6

A: doubly bonded oxygen at BE _ 530.8–531.3 eV, B: singly bonded oxygen in alcohols, ethers, and peroxides at BE _ 531.1–531.3 eV; C: singly bonded oxygen in acids, esters, and hydroperoxides at BE _ 533.3–533.5 eV, D: peroxyacid, peroxyester and/or charge effect at BE _ 534.8–535.2 eV [53–56].

3.2. Theoretical section

A possible model of HPD reaction with a pure carbon NC is shown in Figure 8. Analysis of this scheme indicates that the reaction rate is enhanced by the increasing rate of formation of HO• radicals due to their chemisorption on the carbon surface. The final product of this reaction is an oxidized carbon material:

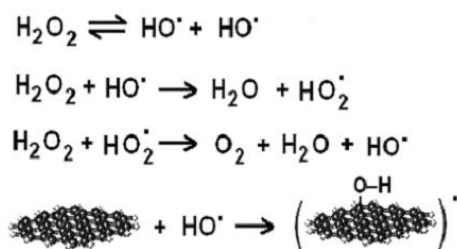


Figure 8. Scheme of H₂O₂ decomposition.

It was found that the interaction of NC with HO[•] radical proceeds in two stages: formation of (1) a physically adsorbed complex and (2) a chemical bond between the reactants after surmounting the energy barrier of transition state. Figure 9 also illustrates how the geometry of the complexes changes in the case of the nitrogen-containing [C₄₀N₂H₁₆] NC. Due to physical adsorption, paramagnetic [[•]OH...NC] complexes are formed, where the HO[•] radical is coordinated to the carbon plane via the hydrogen atom and the electron density is transferred from the π-system of the carbon matrix to the HO[•] radical (Figure 9a). For the [[•]OH...N-NC] system the value of transferred charge does not exceed -0.071 a.u. (Table 4), indicating a weak interaction between the electron systems of the NC and HO[•] radical.

The free energy of the physical adsorption ΔG_{pa} was calculated as

$$\Delta G_{\text{fa}} = \Delta E[\text{OH}^\bullet \dots \text{NC}] - \Delta E[\text{HO}^\bullet] - \Delta E[\text{NC}] \quad (2),$$

where the ΔE are the total energies of the corresponding physically-adsorbed complex [[•]OH...NC], HO[•] radical [HO[•]], and the NC, respectively.

Figure 9 and Table 4 show that the physically adsorbed complex [[•]OH...N-NC] is stronger than [[•]OH...O-NC] due to its lower value of ΔG_{pa}. The adsorption energy ΔG_{pa}, the charge transfer Δρ_{HO}, and the hydrogen bond length *d* between HO[•] radical and the NC plane in these systems correlate with the electron donor capability of the NC studied, in particular with the energy value *E*_{HOMO}, the vertical ionization potential *I*_p of the carbon clusters.

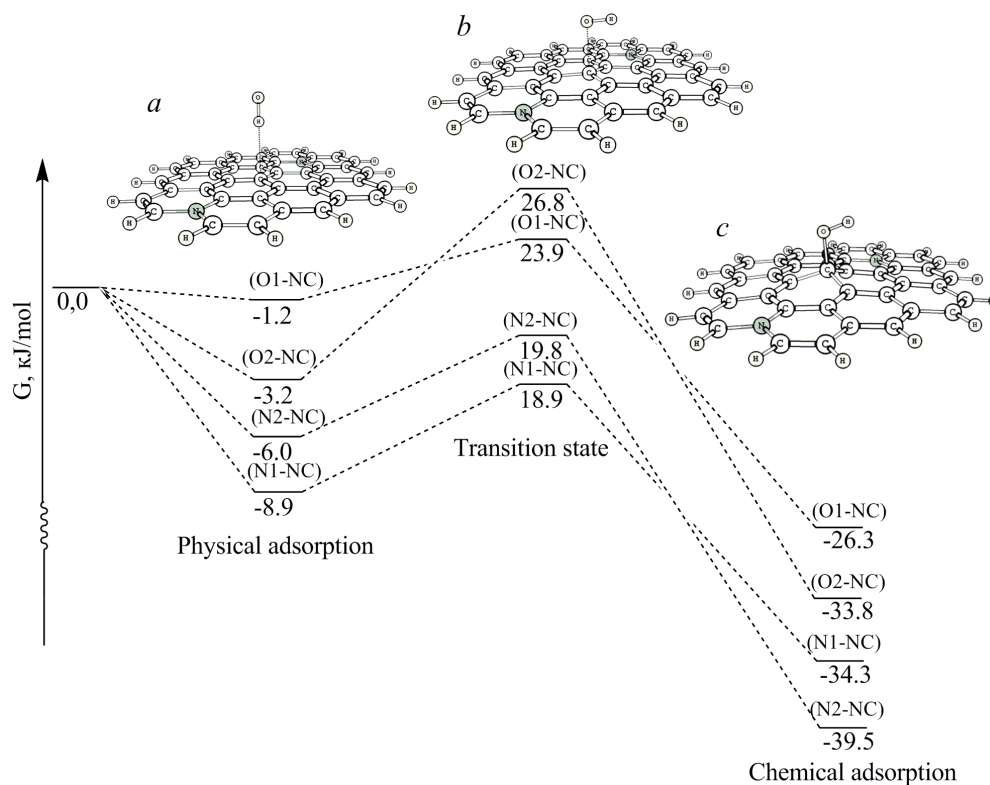


Figure 9. Energy diagram of the interaction between the HO[•] radical and the corresponding NC. G is the Gibbs energy. *a* – physically adsorbed [[•]OH...NC] complexes; *b*: [[•]HO...NC]^{*} transition state structures; *c*: chemically adsorbed [HO-NC][•] complexes.

Table 4. Characteristics of the hydroxyl radical and NC interaction*

Carbon nanocluster	$I_p = E_{HOMO}$ (eV)	$k \cdot 10^{-4}$, s ⁻¹ , pH~8.0	Physical adsorption		[Transition state]			Chemical adsorption			
			$-\Delta G_{pa}$	$-\Delta \rho_{HO\cdot}$	d , Å	ΔG_{ts}	$-\Delta \rho_{HO\cdot}$	iv_{ts} , cm ⁻¹	$-\Delta G_{ca}$	$-\Delta \rho_{HO\cdot}$	$\Sigma \varphi_{C\alpha}$
			kJ/mol			kJ/mol			kJ/mol		
O1-NC	4.773	2.04	1.2	0.0069	2.56	23.9	0.044	443.3	26.3	0.093	340.2
O2-NC	4.063		3.2	0.0052	2.58	26.8	0.052	370.6	33.8	0.093	339.2
N1-NC	3.205	7.83	8.9	0.0705	2.52	18.9	0.092	316.9	34.3	0.129	335.8
N2-NC	4.024		6.0	0.0050	2.50	19.8	0.086	398.6	39.5	0.105	338.6

* I_p : ionization potential, k : rate constant, ΔG : adsorption energy corresponding to the process defined in the subscript, $\Delta \rho_{HO\cdot}$: , d : ; iv_{ts} : wave number of the imaginary vibration mode, $\Sigma \varphi_{C\alpha}$: calculated angular sum; subscripts: pa: physical adsorption, ts: transition state, ca: chemical adsorption.

The chemisorption of the HO[•] radical on the carbon NC passes through the formation of an activated (transition) state [HO[•]...NC]^{*} with simultaneous distancing of hydrogen and approach of oxygen atoms to the plane (Figure 8 *b*). The existence of the transition states is confirmed by the single imaginary vibration mode (*iv_{ts}*). It corresponds to the transition vector with absolute value associated with the energy barrier slope of the potential energy curve. In the transition state complex the hydroxyl radical is coordinated through its oxygen atom.

The activation energy ΔG_{ts} of the HO[•] radical NC interaction in the activated complexes [HO[•]...NC]^{*} were calculated as the difference between the total energies of physically adsorbed structures (Figure 9 *a*) and those of transition state complexes (Figure 9 *b*). The obtained ΔG_{ts} and the imaginary frequency of the normal modes of the transition vectors *iv_{ts}* in the activated complexes decrease with increasing electron donor capability of the NC (Table 4). From the comparison of the calculated ΔG_{ts} values and the experimental rate constants of HPD it was found that the lowest activation energy (~19 kJ/mol) corresponds to the highest rate constant, both found for the N-containing CNT. Additionally, the experimental E_a range is in agreement with the theoretical activation energy ΔG_{ts} from the calculations. As a whole, the minimum values in both cases correspond to low activation energy and fast decomposition of H₂O₂.

Table 4 and Figure 9 show that the activation energy and Gibbs reaction energy of the N-doped NCs is lower than for the oxidized NCs and independent of the position of the heteroatom in the nanocluster.

The formation of the chemisorbed complexes (Figure. 9 *c*) is the final stage of the NC and hydroxyl radical interaction. As Figure 9 shows, the geometrical structures of the activated [HO[•]...NC]^{*} and the chemisorbed [HO–NC][•] complexes are similar. In both cases the HO[•] radical is coordinated with the carbon plane through the oxygen atom. Consequently, the surface of carbon matrix is oxidized and C_α–OH covalent bonds are formed. It has been found that the C_α atom is not co-planar to the carbons of the NC as its calculated angular sum (φ_{C_α}) is less than 360° (Table 4). The hybridization of the C_α atom changes ($sp^2 \rightarrow sp^3$) which results in the reduction of the π -conjugated area and an increase in the ionization potential I_p .

Due to the chemisorption, the negative charge of the OH group increases with a decrease in the ionization potential I_p . The energy effect of the chemisorption reaction of the HO[•] radical on the surface of the [HO–NC][•] complexes ΔG_{ca} was calculated as the difference between the total energies

of the chemo- $[\text{HO-NC}]^{\bullet}$ and physisorbed $[\bullet\text{OH}\dots\text{NC}]$ complexes (Table 4). It was found that the value of ΔG_{ca} of $[\text{HO-N-NC}]^{\bullet}$ is much higher than that of $[\text{HO-O-NC}]^{\bullet}$. Therefore, an O-containing paramagnetic nanocluster formed in the chemisorption is more stable than the N-containing one. These results demonstrate that with rising the electron donor capability of NC the values of ΔG_{ca} decrease. This indicates that desorption of OH groups and regeneration of the surface are easier for the N-NC samples. Consequently, the value of the chemisorption energy ΔG_{ca} can be associated with the operational stability of the samples studied. According to the results of the quantum chemical calculations, the best operation stability should be observed for N-CNT, whilst the worst one is for O-CNT. These results are in good agreement with the experimental data.

4. Conclusions

Oxygen- and nitrogen-containing MWCNTs of similar morphology were exposed to hydrogen peroxide in aqueous medium. Both materials display catalytic performance, as proved by their high rate constants and low activation energies in the reaction studied. The good agreement between the quantum chemical calculation of the HO^{\bullet} radical - carbon plane interaction and the experimental data shows that the model proposed is suitable to describe the HPD catalytic process on CNT surface. The results of the model calculations demonstrate that the catalytic activity of the CNTs in the electron transfer reaction is determined by their electron donor capability. This theoretical investigation helped to reveal the mechanism of H_2O_2 decomposition on the carbon surface. It is found that the end product of the MWCNT catalyzed HPD is an oxidized carbon surface.

Acknowledgements

This work was supported by the EC Seventh Framework Program (FP7/2007-2013).

The quantum chemical calculations were performed on the computational complex of the Chuiko Institute of Surface Chemistry of National Academy of Sciences of Ukraine. The support of the Hungarian National Fund OTKA K101861 is acknowledged.

References

-
1. Carbon materials for catalysis / Ed. by Serp P., Figueiredo J.L. – New Jersey: John Wiley & Sons, Inc, 2009.
 2. *Iijima S.* Helical microtubules of graphitic carbon // *Nature*. – 1991. – Vol. 354. – P.56-58.
 3. *Muradov N.* Catalysis of methane decomposition over elemental carbon // *Catal. Commun.* – 2002. – Vol.2. – P.89-94.
 4. *Luo J.Z., Gao L.Z., Leung Y.L. et al.* The decomposition of NO on CNTs and 1 wt% Rh/CNTs // *Catal. Lett.* – 2000. – Vol. 66. – P. 91-97.
 5. *Yu D., Nagelli E., Du F. et al.* Metal-free carbon nanomaterials become more active than metal catalysts and last longer // *Phys. Chem. Lett.* – 2010. – Vol. 1. – P. 2165-2173.
 6. *Zhang J., Liu X., Blume R. et al.* Surface-modified carbon nanotubes catalyze oxidative dehydrogenation on n-butane // *Science*. – 2008. – Vol. 322. – p. 73-77.
 7. *Su D.S., Maksimova N., Delgado J.J. et al.* Nanocarbons in selective oxidative dehydrogenation reaction // *Catal. Today*. – 2005. – Vol. 102-103. – P.110-114.
 8. *Luo J., Peng F., Yo H. et al.* Aerobic liquid-phase oxidation of ethylbenzene to acetophenon catalyzed by carbon nanotubes // *ChemCatChem*. – 2013. – Vol. 5. – P. 1578 – 1586.
 9. *Nigrovski B., Scholz P., Krech T. et al.* The influence of microwave heating on the texture and catalytic properties of oxidized multi-walled carbon nanotubes // *Catal. Commun.* – 2009. – Vol. 10. – P. 1473-1477.
 10. *Croston M., Langston J., Takacs G. et al.* Conversion of aniline to azobenzene at functionalized carbon nanotubes: a possible case of a nanodimensional reaction // *Int. J. Nanosci.* – 2002. – Vol. 1. – P. 285-293.
 11. *Croston M., Langston J., Sangoi R. et al.* Catalytic oxidation of p-toluidine at multiwalled functionalized carbon nanotubes // *Int. J. Nanosci.* – 2002. – Vol.1. – P.277- 283.
 12. *Luo J., Peng F., Wang H. Et al.* Enhancing the catalytic activity of carbon nanotubes by nitrogen doping in the selective liquid phase oxidation of benzyl alcohol // *Catal. Commun.* – 2013. – Vol. 39. – P. 44 – 49.
 13. *Yang S., Li X., Zhu W. et al.* Catalytic activity, stability and structure of multi-walled carbon nanotubes in the wet air oxidation of phenol // *Carbon* – 2008. – Vol.46. – P.445-452.
 14. *Yang S., Zhu W., Li X. et al.* Multi-walled carbon nanotubes (MWCNTs) as an efficient catalyst for catalytic wet air oxidation of phenol // *Catal. Commun.* – 2007. – Vol. 8. – P. 2059-2063.
 15. *Fazio E., Piperopoulos E., Hameed A.R.S. et al.* Correlation between carbon nanotube microstructure and their catalytic efficiency towards the p-coumaric acid degradation // *Curr. App. Phys.* – 2013. – Vol. 13. – P. 748 -752.
 16. *Milone C., Hameed A.R.S., Piperopoulos E. Et al.* Catalytic wet air oxidation of p-coumaric acid over carbon nanotubes and activated carbon // *Ind. Eng. Chem. Res.* – 2011. – Vol. 50. – P. 9043-9053.
 17. *Cao Y., Yu H., Tan J. et al.* Nitrogen-, phosphorous- and boron-doped carbon nanotubes as catalysts for the aerobic oxidation of cyclohexane // *Carbon*. – 2013. – Vol. 57. – P. 433 – 442.
 18. *Yu H., Peng F., Tan J. et al.* Selective catalysis of the aerobic oxidation of cyclohexane in the liquid phase by carbon nanotubes // *Angew. Chem. Int. Ed.* – 2011. – Vol. 50. – p. 3978-3982.
 19. *Gonçalves A.G., Figueiredo J.L., Orfao J.J.M. et al.* Influence of the surface chemistry of multi-walled carbon nanotubes on their activity as ozonation catalysts // *Carbon*. – 2010. – Vol. 48. – P. 4369-4381.

-
20. Liu Z.-Q., Ma J., Cui Y.-H. *et al.* Influence of different heat treatments on the surface properties and catalytic performance of carbon nanotube in ozonation // *Appl. Catal. B: Environ.* – 2010. – Vol. 101. – P. 74–80.
 21. Chizari K., Deneuve A., Ersen O. *et al.* Nitrogen-doped carbon nanotubes as a highly active metal-free catalyst for selective oxidation // *ChemSusChem.* – 2012. – Vol. 102-108.
 22. Kang Z.H., Wang E.B., Mao B.D. *et al.* Heterogeneous hydroxylation catalyzed by multi-walled carbon nanotubes at low temperature // *Appl. Catal. A.* – 2006. – Vol. 299. – P. 212-217.
 23. Dommele S., Jong K.P., Bitter J.H. Nitrogen-containing carbon nanotubes as solid base catalysts // *Chem. Commun.* – 2006. – Vol. P. 4859–4861.
 24. Hu X., Wu Y., Zhang Z. CO oxidation on metal-free nitrogen-doped carbon nanotubes and the related structure-reactivity relationships // *J. Mater. Chem.* – 2012. – Vol. 22. – P. 15198-15205.
 25. Datsyuk V., Kalyva M., Papagelis K. *et al.* Chemical oxidation of multiwalled carbon nanotubes // *Carbon.* – 2008. – Vol. 46. – P.833-840.
 26. Wang Y.H., Shan H.W., Hauge R.H. *et al.* A highly selective, one-pot purification method for single-walled carbon nanotubes // *J. Phys. Chem. B.* – 2007. – Vol. 111. – P. 1249–1252.
 27. Magera M., Accorsi G., Meneghetti M. *Et al.* Cap removal and shortening of double-walled and very-thin multi-walled carbon nanotubes under mild oxidative condition // *Carbon.* – 2009. – Vol. 47. – P. 675-682.
 28. Oliveira L.C.A., Silva C.N., Yoshida M.I. *et al.* The effect of H₂ treatment on the activity of activated carbon for the oxidation of organic contaminants in water and the H₂O₂ decomposition // *Carbon.* – 2004. – Vol. 42. – P.2279-2284.
 29. Khalil L.B., Girgis B.S., Tawfik T.A. Decomposition of H₂O₂ on activated carbon obtained from olive stone // *J. Chem. Technol. Biochem.* – 2001. – Vol. 76. – P. 1132-1140.
 30. Voitko K.V., Whitby R.L.D., Gun'ko V.M. *et al.* Morphological and chemical features of nano and macroscale carbons affecting hydrogen peroxide decomposition in aqueous media // *J. Coll. Inter. Sci.* – 2011. – Vol. 361. – P. 129-136.
 31. Strelko V.V., Kartel N.T., Duchno I.N. *et al.* Mechanism of reductive oxygen adsorption on active carbons with various surface chemistry // *Surf. Sci.* – 2004. – V. 548 – P. 281–290.
 32. Strelko V.V., Kuts V.S., Thrower P.A. On the mechanism of possible influence of heteroatoms of nitrogen, boron and phosphorus in a carbon matrix on the catalytic activity of carbons in electron transfer reaction // *Carbon.* – 2000. – V. 38. –P. 1499–1503.
 33. Radovic L.R. *Chemistry and physics of carbon.* – New York: Marsel Dekker, 2001.
 34. Sugano M., Ikemizu R., Mashimo K. Effects of the oxidation pretreatment with hydrogen peroxide on the hydrogenolysis reactivity of coal liquefaction residue // *Fuel Proc. Tech.* – 2002 – V. 77–78. – P. 67–73.
 35. Balbuena P.B., Calvo S.R., Lamas E.J. *et al.* Adsorption and dissociation of H₂O₂ on Pt-and Pt-alloy clusters and surface // *J. Phys. Chem. B.* – 2006. – V. 110. – P. 17452–17459.
 36. Brichka S.Ya., Prikhod'ko G.P., Sementsov Yu.I. *et al.* Synthesis of carbon nanotubes from a chlorine-containing precursor and their properties // *Carbon.* – 2004. – Vol. 44. – P. 2581-2587.
 37. Wang Z., Shirley M.D., Meikle S.T. *et al.* The surface acidity of acid oxidised multi-walled carbon nanotubes and the influence of in-situ generated fulvic acids on their stability in aqueous dispersions // *Carbon.* – 2009. – Vol. 47. – P. 73-79.
 38. Everett H.D. Reporting data on adsorption from solution at the solid/solution interface // *Pure & Appl. Chem.* – 1986. – Vol. 58. – P. 967-984.

-
39. *László K, Tombácz E, Kerepesi P.* Surface chemistry of nano-porous carbon and the effect of pH on adsorption from aqueous phenol and 2,3,4-trichlorophenol solutions // *Coll. Surf. A.* – 2003. – Vol. 230. – P. 13–22.
40. *Hu X., Wu Y., Li H. et al.* Adsorption and activation of O₂ on nitrogen-doped carbon nanotubes // *J. Phys. Chem. C.* – 2010. – Vol. 114. – P. 9603–9607.
41. *Hu X., Liu C., Wu Y. et al.* Density functional theory study on nitrogen-doped carbon nanotubes with and without oxygen adsorption: the influence of length and diameter // *New J. Chem.* – 2011. – Vol. 35. – P. 2601–2606.
42. *Becke A.D.* Density functional thermochemistry. III. The role of exact exchange // *J. Chem. Phys.* – 1993. – V. 98. – P. 5648–5653.
43. *Lee C., Yang W., Parr R.G.* Development of the Colle-Salvetti correlation-energy formula into a functional of the electron density // *Phys. Rev. B.* – 1988. – V. 37. – P. 785–789.
44. *Grimme S., Ehrlich S., Goerigk L.* Effect of the damping function in dispersion corrected density functional theory // *J. Comp. Chem.* – 2011. – Vol. 32. – P. 1456–1465.
45. *Schmidt W., Baldrige K.K., Boatz J.A. et al.* General atomic and molecular electronic-structures system: Review // *J. Comp. Chem.* – 1993. – V. 14. – P. 1347–1363.
46. *Wales D.J., Berry R.S.* Limitations of the Murrell-Laidler theorem // *J. Chem. Soc. Faraday Trans.* – 1992. – V. 88. – P. 543–544.
47. *Jensen F.* Introduction to computational chemistry. – New York: Wiley, 2006. – 624 p.
48. *Wepasnick K.A., Smith B.A., Schrote K.E. et al.* Surface and structural characterization of multi-walled carbon nanotubes following different oxidative treatments // *Carbon.* – 2011. – Vol. 49. – P. 24–36.
49. *Wang X.X., Wang J.N.* Preparation of short and water-dispersible carbon nanotubes by solid-state cutting // *Carbon.* – 2008. – Vol. 46. – P. 117–125.
50. *Lee S., Kim H., Lee J. et al.* Donor and acceptor-like electronic states in a one-dimensional semiconductor // *Surface Science.* – 2006. – Vol. 600(22). – P. 4937–4940.
51. *Glevatska K.V., Bakalinska O.M., Tarasenko Y.O. et al.* Catalytic (enzyme-like) properties of multi-layer carbon nanotubes // *Kharkov University Bulletin.* – 2010. – Vol. 895 (18). – P. 245–255.
52. *W. Shen, Z. Li, Y. Liu,* *Chem. Eng.* 1 (2008) 27–40.
53. *D. Rosenthal, M. Ruta, R. Schlogl, L. Kiwi-Minsker,* *Carbon* 48 (2010) 1835–1843.
54. *S. Tanuma, C.J. Powell, D.R. Penn,* *Surf. Interface Anal.* 20 (1993) 77–89.
55. *S. Yumitori,* *J. Mater. Sci.* 35 (2000) 139–146.
56. *S. Biniak, G. Szymanski, J. Siedlewski,* *Carbon* 35 (1997) 1799–1810.